Abrupt and Gradual Extinction Among Late Permian Land Vertebrates in the Karoo Basin, South Africa

Peter D. Ward,[1]* Jennifer Botha,[3] Roger Buick,[2]
Michiel O. De Kock,[5] Douglas H. Erwin,[6] Geoffrey H. Garrison,[2]
Joseph L. Kirschvink,[4] Roger Smith[3]

The Karoo basin of South Africa exposes a succession of Upper Permian to Lower Triassic terrestrial strata containing abundant terrestrial vertebrate fossils. Paleomagnetic/magnetostratigraphic and carbon-isotope data allow sections to be correlated across the basin. With this stratigraphy, the vertebrate fossil data show a gradual extinction in the Upper Permian punctuated by an enhanced extinction pulse at the Permian-Triassic boundary interval, particularly among the dicynodont therapsids, coinciding with negative carbon-isotope anomalies.

The Permian extinction is universally portrayed as the most catastrophic of all Phanerozoic mass extinctions (1), yet its cause remains problematic. Various hypotheses include climate change due to increased atmospheric CO_2 and/or CH_4 (2), the effects of extraterrestrial impact (3–5), the effects of the eruption of the Siberian Traps, and some synergistic combination of these (6), among others. An important test of any mechanism is a consideration of the pattern of extinctions. The marine extinctions are well described in several areas, notably Meishan, China (7). Here, we report new chemostratigraphic, biostratigraphic, and magnetostratigraphic data from multiple stratigraphic sections located in the Karoo basin of South Africa that provide an exceptionally detailed record of the terrestrial extinctions.

Permian-Triassic (P-T) strata in the central Karoo basin provide the most intensively investigated record of vertebrate fossils from

[1]Department of Biology, [2]Department of Earth and Space Sciences, University of Washington, Seattle, WA 98195, USA. [3]Karoo Paleontology, Iziko: South African Museum, Cape Town, South Africa. [4]Division of Geological and Planetary Sciences, California Institute of Technology, Pasadena, CA 91125, USA. [5]Department of Geology, Rand Afrikaans University, Johannesburg, South Africa. [6]Department of Paleobiology, MRC-121 Smithsonian Institution, Washington, DC 20013, USA.

*To whom correspondence should be addressed. E-mail: argo@u.washington.edu

the Upper Permian through the Triassic (*8*). These strata are dominantly fluvial overbank sediments deposited near the center of a subsiding retroarc foreland basin (*9*). We have sampled across 200 m of the Palingkloof Member of the Balfour Formation and the overlying Katberg Formation, where we recognize four units spanning the Upper Permian and Lower Triassic (*10*). Fossils were collected from these strata at five different areas. Hence, correlating the sections, which is difficult between fluvial sections and has been notably problematic in the Karoo (*11*), is critical.

To correlate the stratigraphy, we obtained a magnetostratigraphic record (Fig. 1) (*12*) from three sections [some data are also in (*13*)]. Samples from Unit II and Unit III are all of normal polarity (Chron N1), and we identified a reversed polarity magnetozone (R1) ~5 m beneath the Unit I-II contact (*14*). At Lootsberg and Wapadsberg, the normal-polarity zone extends well up into the Katberg Formation (Unit IV). At Lootsberg, where the youngest strata were sampled of all the sections, there is a change to reversed polarity (R2) above about 130 m and a final switch back to normal (N2) at the top. Given paleontological constraints (*8*), we correlate the long normal found in Units II, III, and most of IV with magnetozone SN1 of the classic German Trias sections (*15*) and thus define the top and bottom of the Griesbachian stage in the Karoo. The superjacent reversal at Lootsberg Pass is most parsimoniously correlated with magnetozone SR1 of central Germany, R2 of the Southern Alps, and GR1 of the Canadian Arctic. Although there is some uncertainty about the reversal pattern near the P-T boundary (*16*), recent records in Europe suggest that the boundary occurs just above the base of a reversed-to-normal-polarity transition in Germany, although there has been a recent report placing it slightly lower, in the uppermost part of the reversed chron (*17*). The base of Unit II is thus approximately coincident with the P-T boundary.

These correlations were tested by measuring sedimentary carbon isotope ($\delta^{13}C_{carb}$ and $\delta^{13}C_{org}$) stratigraphy at all the sections at meter or submeter sampling frequency (*12*) (Fig. 2), a finer resolution than has been done before (*18*). This earlier P-T isotope study in the Karoo found a single negative $\delta^{13}C_{carb}$ excursion approximately coincident with the last occurrence of the latest Permian

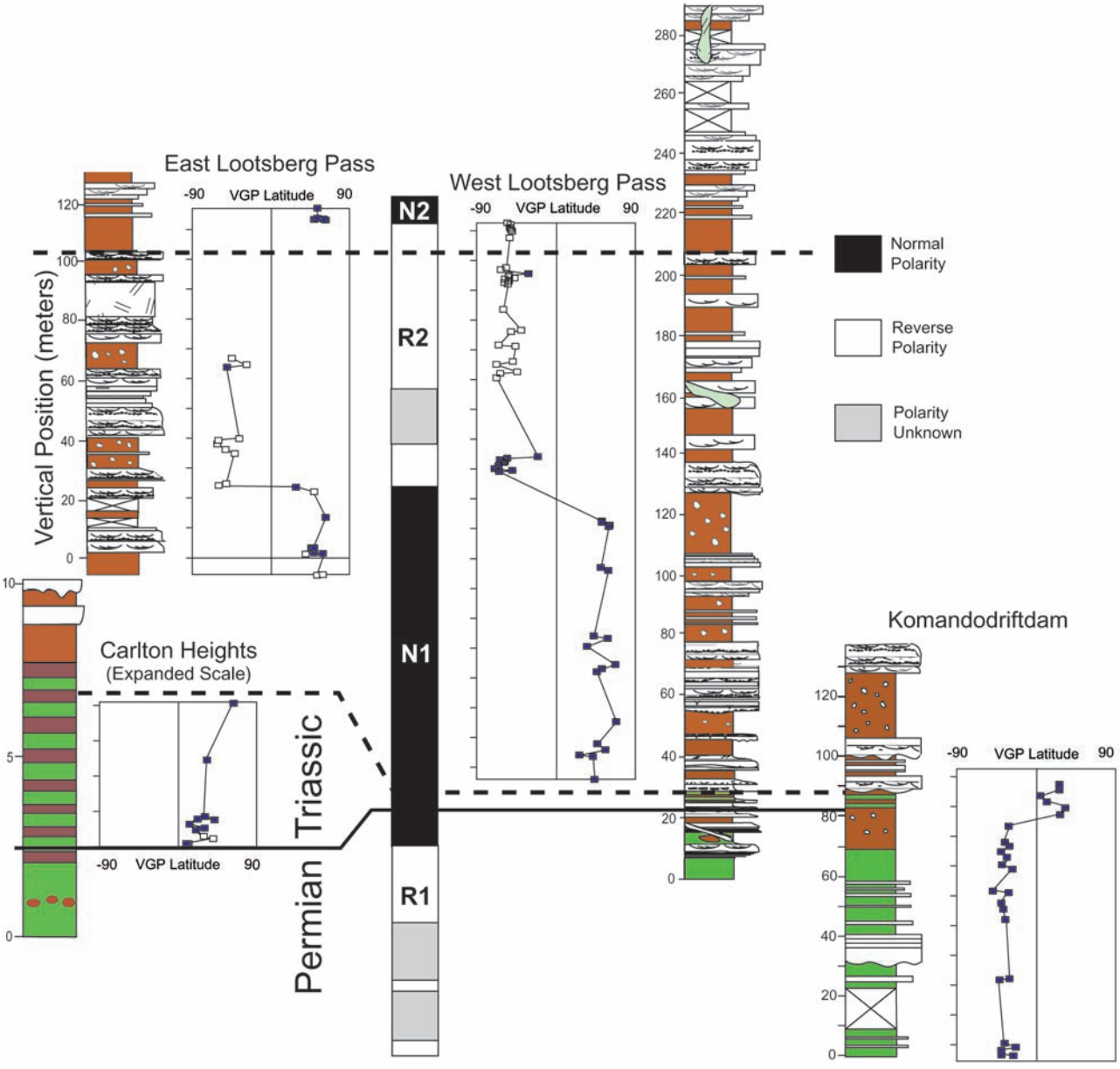

Fig. 1. Magnetostratigraphic correlation across the Karoo basin. The dashed lines represent the correlated positions between the stratigraphic sections.

zonal index fossil *Dicynodon*. The global $\delta^{13}C$ record for the P-T boundary period is known in varying detail from several dozen marine and fewer nonmarine sites (e.g., *19, 20*). Intensively sampled sections show a gradual decline in the sedimentary $^{13}C:^{12}C$ ratio upward through the Upper Permian, then a sudden decline of >2‰ at or near the paleontologically defined extinction boundary, followed by a gradual increase in $\delta^{13}C$. The sudden $\delta^{13}C$ decline precedes the formal P-T boundary based on the first occurrence of the Triassic conodont *Hindeodus parvus* at the global stratotype section and point (GSSP) P-T stratotype in Meishan, China, where the boundary has been placed at Bed 27. At Meishan, the lowest $\delta^{13}C$ values are found in Bed 25 (*7*), coincident with the level of maximal species disappearance (94% loss of then-extant marine invertebrates). Thus, the mass extinction and sharp negative excursion in $\delta^{13}C$ are slightly older than the formal stratigraphic boundary.

We sampled both bulk sediment and carbonate paleosol nodules for carbon isotope stratigraphy from our measured sections. Soil carbonate $\delta^{13}C$ ($\delta^{13}C_{carb}$) is a function of both the $\delta^{13}C$ of atmospheric CO_2 ($\delta^{13}C_{CO2}$) and the partial pressure of CO_2 in the atmosphere (pCO_2), and thus soil $\delta^{13}C_{carb}$ records can be more scattered than marine $\delta^{13}C_{carb}$ records (*21*). Nevertheless, the $\delta^{13}C_{carb}$ results show a prominent drop within Unit I that is consistent with our assessment that Unit I/Unit II contact marks the P-T extinction (Fig. 2). The $\delta^{13}C_{carb}$ values maintain a broad minimum in Unit II, a pattern similar to global marine $\delta^{13}C_{carb}$ records. The lowermost negative excursion in $\delta^{13}C_{carb}$ observed in the Karoo most parsimoniously correlates with the singular, lower Griesbachian negative $\delta^{13}C_{carb}$ excursion reported recently from a Late Permian–Late Triassic carbonate platform in the Nanpanjiang Basin, Guizhou Province, China (*22*). Furthermore, the broad swings in $\delta^{13}C_{carb}$ values that were measured higher in the Karoo sections (Fig. 2) appear to be consistent with Smithian and Spathian age $\delta^{13}C_{carb}$ excursions in the same marine $\delta^{13}C_{carb}$ record.

The bulk sedimentary organic carbon isotope records ($\delta^{13}C_{org}$) from the Carlton Heights and Lootsberg sections provide further support for these conclusions (Fig. 2). The data also supports the magnetostratigraphic correlation of Unit II between the northern (Carlton Heights and Bethulie regions) and southern (Lootsberg and Wapadsberg regions) parts of the basin. At the Carlton Heights and Lootsberg sections, $\delta^{13}C_{org}$ decreases from ~ –24‰ Vienna Pee Dee belemnite (VPDB) to ~ –26‰ VPDB across the uppermost meter of Unit I and remains there through Unit II and into Unit III. Between 15 m and 22 m (Unit III), $\delta^{13}C_{org}$ increases in both sections to ~ –21‰ and then decreases ~1‰ at the base of Unit IV. This pattern is typical of P-T $\delta^{13}C$ records measured elsewhere in the world. The Wapadsberg and Bethulie $\delta^{13}C_{org}$ records do not show any substantial negative excursions, particularly not at the P-T boundary, but both of these sections are extensively intruded by Mesozoic dolerite dikes and sills. We suggest that this igneous activity has homogenized the primary $\delta^{13}C_{org}$ record at these two sections.

Fossil vertebrate biostratigraphy confirms that Unit II is essentially contemporaneous across the Karoo basin. At all sections, the highest occurrence of the uppermost Permian zonal index, *Dicynodon lacerticeps*, is found either immediately below (at the fossiliferous Lootsberg, Wapadsberg, and Bethulie sections) or at most several meters below the base of Unit II (at the fossil-poor Carlton Heights and Kommandodrift Dam sections). *Dicynodon lacerticeps* was never found in or above Unit II, and the first Triassic fossil common to all sections—*Lystrosaurus* sp. C—was found in the lower strata of Unit III but never in Unit II.

In summary, three independent correlation methods support our contention that Unit II is both essentially isochronous across the Karoo basin and also time equivalent with the P-T boundary in China. This allows us to use this unit as a datum surface against which our vertebrate range taxa can be plotted and to compare the patterns of extinction with those observed at other P-T sections.

Over a period of 7 years, we collected 126 skulls assigned to 21 vertebrate taxa from the sections shown here (reptile or amphibian) (Fig. 3) (*23*). We treat these taxa as species, although further study will probably result in an even greater number of taxa. We found 13 taxa in Unit I (Upper Permian), only 4 of which persist into Unit II, and 12 taxa in Units II to IV. Six of the 13 taxa

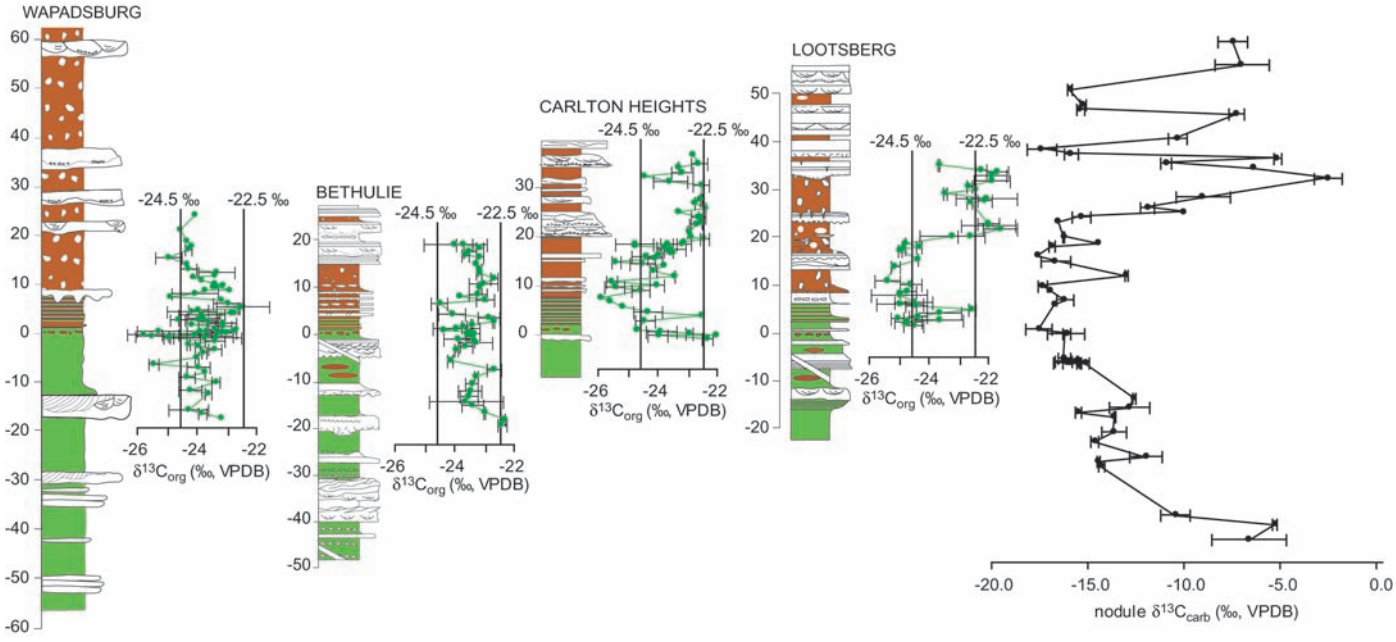

Fig. 2. The combined soil nodule $\delta^{13}C_{carb}$ record and individual lithologic and $\delta^{13}C_{org}$ records for four sections in the Karoo basin. The two sections at left (Wapadsburg, southern basin; Bethulie, northern basin) have been strongly affected by heating, as evidenced by a lack of primary paleomagnetic signal from either section. The results from Carlton Heights and Lootsberg Pass, however, have similar negative $\delta^{13}C_{org}$ excursions within Unit II, followed by an increase in $\delta^{13}C_{org}$ values in Units III and IV. The $\delta^{13}C_{carb}$ curve at the far right is combined data from carbonate nodules obtained from the Carlton Heights and the Lootsberg regions.

found in Unit I show their last appearance datums (LADs) in the last 10 m of Unit I, which suggests an enhanced rate of extinction in the latest Permian. These range terminations occurred either before or simultaneously with the reduced $\delta^{13}C_{org}$ values toward the top of Unit I.

Incomplete preservation or collection failure can make abrupt extinctions look gradual, i.e., the Signor-Lipps effect (*24*, *25*), so the assumption of simultaneous extinction of the included taxa was tested using the Kolmogorov-Smirnov (K-S) goodness-of-fit test (*26*). The case for the Karoo basin is complicated, because some of our sampled taxa (i.e., *Pristerodon* sp. and *Aelurognathus* sp.) might have become extinct before the base of Unit II or long after (*Ictidosuchoides* sp., *Thrinaxodon* sp., *Lystrosaurus* sp. C.), thereby complicating the statistical protocols (*27*). Thus, we calculated confidence intervals on stratigraphic ranges (*28*). We chose 20% confidence intervals following the improved method for testing extinction levels (*29*) for each of the nine taxa (Table 1).

Four taxa (*Theriognathus* sp., *Dicynodon lacerticeps*, *Lystrosaurus* sp. A, and *Rubidgea* sp.) appear to have become extinct at or near the base of Unit II (Fig. 3). We are also confident that *Pristerodon*, *Aelurognathus*, and the abundant and widespread taxon *Diictodon* sp. were extinct before deposition of Unit II, whereas the taxa *Lystrosaurus* sp. B, *Moschorhinus* sp., and *Owenetta* sp. became extinct during, or soon after, the initiation of sedimentation marking the Katberg Formation (Unit IV) (Fig. 3). The 90% confidence interval on the position of the mass extinction extends from 0 m (stippled level A) to about 20 m, or from the base of Unit II up into the middle part of Unit III. Thus, there is a low probability that the mass extinction of the Karoo vertebrates occurred within the Katberg Formation (stippled level B), where the mass extinction has been traditionally placed (*30*).

We have also used confidence intervals to examine the origination of taxa. Theoretically, if the majority of Permian extinctions occurred at a specific horizon, we would expect to observe, after the extinction, a follow-on origination of new species into vacated niches (or immigration into the basin). We do not observe this. By inverting the procedure for fossil disappearances, we calculated 20% range extensions downward and from this computed a 94% probability confidence interval for origination (Fig. 3). The results suggest it is probable that at least some species originated before the deposition of Unit II, whereas others originated during and after Unit II deposition. The distribution of originating taxa fails the K-S test for random distribution of new taxa at the 99% level, suggesting that Triassic taxa origination was in response to some event that occurred before the end of the Permian. We caution that new taxa origination may violate the assumption of equal probability of preservation, because new taxa are likely to be rare and uncommon. This effect may overestimate the calculated ranges for originations.

A further caveat is that we are implicitly accepting an empty-niche model brought about by the extinction, even though some or many niches may have been reconstructed

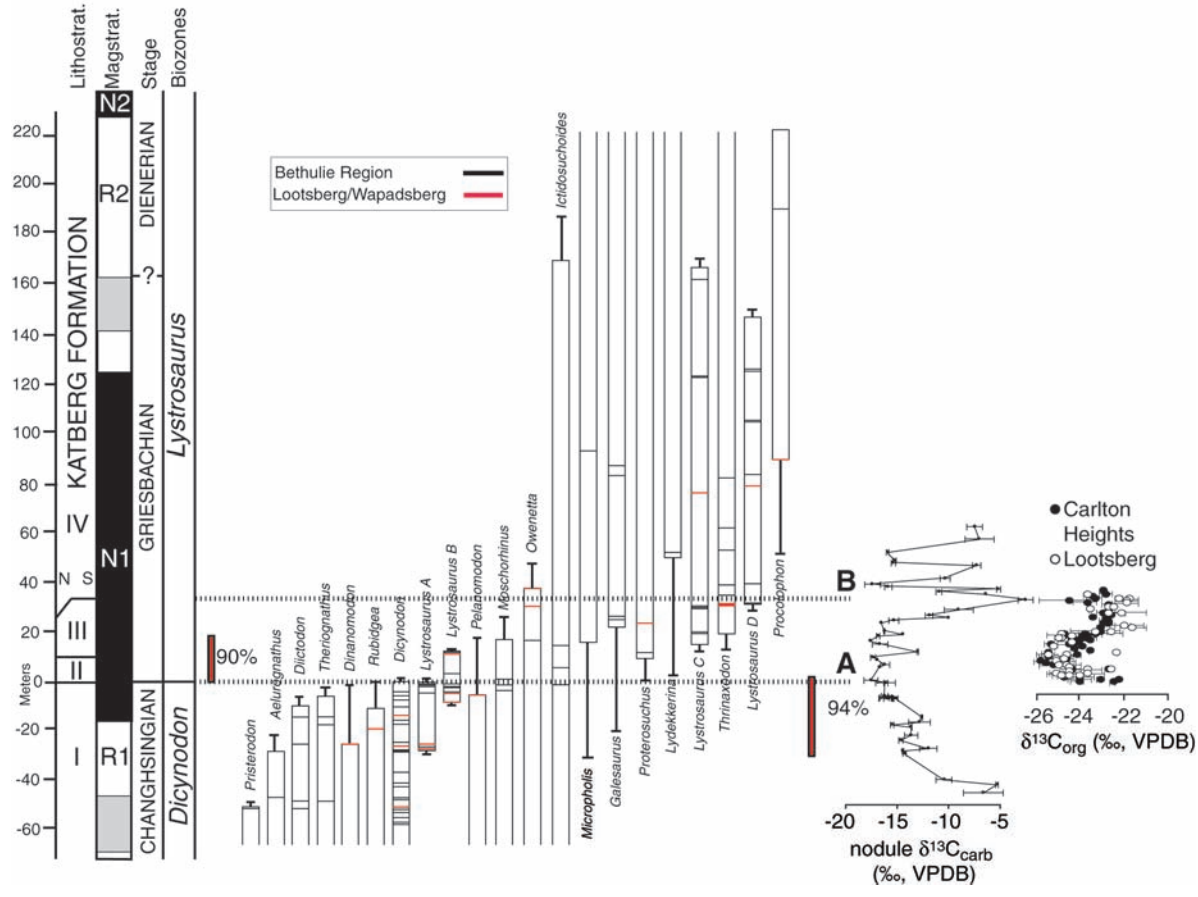

Fig. 3. Magnetostratigraphic, biostratigraphic, and carbon isotopic records from the Karoo basin. This figure can be compared with the generic range chart for the entire Permian/Lower Triassic sequence in the study area (*12*). The red bar on the left is the 90% confidence interval for Permian taxa extinction; the red bar on the right is the 94% confidence interval for Triassic taxa origination, assuming that originations were in response to catastrophic extinction. Level A is the base of Unit II, which is correlated to the highest occurrence of Permian index fossil *Dicynodon lacerticeps*. Level B is the base of Unit IV (Katberg Formation), where a spike in fungal spore abundance and the P-T boundary have been recorded previously (*32*). Of particular note is the appearance of *Lystrosaur* A and *Lystrosaur* B below the P-T boundary. *Lystrosaurs* are Triassic animals, and the appearance of two species below the P-T boundary is evidence that major evolutionary changes were under way before the end of the Permian.

and not refilled. The pattern of extinction and origination appears to be consistent with an enhanced rate of extinction coincident with or just below Unit II, but the number of extinct species there may be no more than five (eight species become extinct in Unit I). The most thorough compilation of the vertebrate record from the *Dicynodon* Zone in the Karoo (*8*) shows that 10 of 21 taxa present at the base of the ~300-m-thick zone are absent in its upper third, indicating that considerable extinction is occurring throughout the zone and not just at its top (*31*). This observation can be supported by replotting known vertebrate ranges in the Karoo such that last occurrences are sequential (*12*), based on the new data presented here and range data from lower zones (*8*). The resulting figure (fig. S4) shows what appears to be a change from an approximately constant background extinction (as recognized by the number of taxa disappearing per unit thickness of strata) below the uppermost Permian, with enhanced extinction in the *Dicynodon* Zone culminating at the P-T extinction pulse at the top of Unit I. In the Lower Triassic–aged *Lystrosaurus* Zone, there is a reduced extinction rate high in Unit II and in Unit III. Two patterns are thus apparent: gradual extinction leading up to the P-T and a pulse of even higher extinction marking the boundary. This pattern is visible both at the species level (Fig. 3) and at the generic level (fig. S4) and is also observed at Meishan among invertebrate marine fossils.

We thus suggest that factors other than the sudden extinction of taxa stimulated the origination or appearance (through emigration) of new Triassic species into the basin. Our statistical inference (and the discovery of *Lystrosaurus* sp. A and B) that Triassic vertebrate fauna may have predated the main Permian extinction pulse is unlike the pattern of mammalian radiation after the Cretaceous-Paleogene (K-P) extinction, the only clear example of a mass extinction associated with a major impact event. The pattern that we observe for the P-T is consistent with a long-term deterioration of the terrestrial ecosystem, with a heightened pulse of both extinction and origination approximately coincident with the P-T boundary.

Unfortunately, the ranges of Permian and Triassic fossil plant remains in our study sections add little information about the pattern of extinction in the Karoo basin or about the relative timing of extinction among plants and animals there. A recent palynological study at Carlton Heights (*32*) identified a spike in fungal spore abundance at the base of our Unit IV (the Katberg Formation) and claimed the fungal spike to be the top of the *Dicynodon* Zone and thus the P-T boundary. However, the study provided insufficient information to ascertain whether the base of Unit IV is Permian or Triassic in age based on palynomorphs (*33*), and we have found in all of our sections, including the site in question, that the Katburg Formation begins well above the top of the Permian.

We interpret the biostratigraphic data presented here as consistent with a period of environmental stress during the latest Permian in this basin, punctuated by a short interval of even greater perturbation, i.e., a long "press" with one (or more) pulses superimposed. A single proximal cause might explain the extinction patterns, such as long-term environmental degradation having reached a critical threshold that triggered a short-term extinction event through ecosystem collapse. Alternatively, the long- and short-term effects observed in the Karoo could have two (or more) different causes. We searched for evidence of an end-Permian bolide impact, such as the impact clays and ejecta layers found commonly in the environmentally similar Hell Creek Formation (Late Cretaceous), Montana, which are associated with the Chicxulub K-P impact. Neither our search nor previous searches in the Karoo sections for minerals associated with large-body impact (*34*) have met with success, although fluvial facies can contain hiatuses and the absence of impact evidence must be tempered with caution.

The P-T southern Karoo basin and the K-P Hell Creek Formation strata were deposited by similar fluvial systems, and they can be compared. The Hell Creek vertebrate paleontological record is constantly diverse up through the last Cretaceous zone, followed by a catastrophic extinction coeval with a negative excursion in the $\delta^{13}C$ record (*35*, *36*) and clear sedimentological and mineralogical evidence of a large-body impact; $\delta^{13}C$ returns to pre-event values within a narrow stratigraphic interval (*35*). The Karoo record is entirely different, and we conclude that if an impact occurred at all, it had a minor role in the end-Permian extinctions in the Karoo. The geologic data from the Karoo are consistent with a more protracted catastrophic ecosystem collapse than a sudden impact would produce.

Table 1. Confidence that vertebrates became extinct or originated prior to deposition of lithological Unit II by application of the equation $C = 1 - (G/R + 1)^{-(H-1)}$, where G is the interval between the highest occurrence of the taxon and the base of Unit II, R is the taxon's observed stratigraphic range, and H is the number of fossiliferous strata within the range of R (*28*). The null hypothesis of a random distribution of fossil horizons is rejected. Taxon confidence (C), extinction before deposition of Unit II. Confidence, origination before deposition of Unit II.

Taxon	Confidence (C) (extinction before deposition of Unit II)	Confidence (origination before deposition of Unit II)
Pristerodon sp.	0.875	
Aelurognathus sp.	0.5	
Diictodon sp.	0.52	
Theriognathus sp.	0.31	
Rubidgea sp.	0.2	
Dicynodon lacerticeps	0.17	
Lystrosaurus sp. *A*	0.13	
Lystrosaurus sp. *B*	0	
Pelanomodon sp.	.05	
Moschorhinus sp.	0	
Owenetta sp.	0	
Ictidosuchoides sp.	0	
Micropholis sp.		0.08
Galesaurus sp.		0.2
Proterosuchus sp.		0.25
Lydekkerina sp.		0.21
Lystrosaurus sp. C		0.69
Micropholis sp.		0.08
Thrinaxodon sp.		0.55
Procolophon sp.		0.54

References and Notes

1. D. H. Erwin, *Nature* **367**, 231 (1994).
2. A. Knoll *et al.*, *Science* **273**, 452 (1996).
3. L. Becker *et al.*, *Science* **291**, 1530 (2001).
4. A. R. Basu *et al.*, *Science* **302**, 1388 (2003).
5. L. Becker *et al.*, *Science* **304**, 1469 (2004).
6. M. J. Benton, R. J. Twitchett, *Trends Ecol. Evol.* **18**, 358 (2003).
7. Y. G. Jin *et al.*, *Science* **289**, 432 (2000).
8. B. Rubidge, *Geol. Surv. S. Afr. Biostratigraphy* **1**, (1995).
9. O. Catuneanu *et al.*, *Basin Res.* **10**, 417 (1998).
10. Two sections were sampled near Lootsberg Pass (S31, 51.005; W24, 52.299, and S31, 49.334; W24, 48.565), one section near Wapadsberg Pass (S31, 52.474; W24, 54.882), one section near Carlton Heights (S30, 35.425; W25, 439.135), one section near Kommandodrift Dam (S31, 76.506; W24, 49.980), and two sections near Bethulie (S30, 24.989; W26, 17.234, and S30, 26.675; W26, 18.006). Four lithostratigraphic facies are present: Unit I, dark gray to gray mudstones, siltstones, and sandstones with sedimentary structures typical of meandering river deposits; strata show rubification in the uppermost meters. Unit II, 3- to 5-m-thick, rhythmically bedded laminated mudrock, described as an event bed (*37*). Unit III, red concretionary mudstone and thin sandstone. Unit IV (Katberg Formation), thick olive-green sandstone with conglomeratic bases interbedded with thinner red siltsone and mudstone; sandstones have sedimentary structures typical of braided river deposits.

11. G. Retallack et al., Geol. Soc. Am. Bull. 115, 1133 (2003).
12. Materials and methods are available as supporting material on Science Online.
13. M. O. de Kock, J. L. Kirschvink, Gond. Res. 7, 175 (2004).
14. All samples passed tests for baked contact, class B reversal, and magnetostratigraphic consistency. The reversal in the upper part of Lootsberg Pass was corroborated at a second parallel section 1 km to the east, where a reversal of similar thickness was found at the same stratigraphic horizon. We have used this pattern to correlate and subdivide the Katberg Formation across the Karoo basin.
15. M. Szurlies et al., Earth Planet. Sci. Lett. 212, 263 (2003).
16. M. Steiner et al., J. Geophys. Res. 94, 7343 (1989).
17. J. Nawrocki, Terra Nova 16, 139 (2004).
18. K. G. MacLeod et al., Geology 24, 227 (2000).
19. M. J. De Wit et al., J. Geol. 110, 227 (2002).
20. W. T. Holser, M. Margaritz, Geochim. Cosmochim. Acta 56, 3297 (1992).
21. T. E. Cerling, Global Biogeochem. Cycles 6, 307 (1992).
22. J. L. Payne, Science 305, 506 (2004).
23. The actual P-T boundary is defined by the base of the Triassic system or the first appearance of the conodont H. parvus in marine strata. The base of the Triassic cannot be identified in the Karoo until a terrestrial index fossil is formally chosen. At present, we have placed the P-T boundary at the level of the highest Permian taxon, a practice that runs contrary to accepted stratigraphic procedure. Here, each taxon is treated as a species; we realize that taxonomic study of each is required. Pending the formal systematic treatment of Lystrosaurus (38), we designate the four separate species of Lystrosaurus from our study area as Lystrosaurus sp. A, B, C, and D.
24. P. W. Signor III, J. H. Lipps, Geol. Soc. Am. Spec. Pap. 190, 291 (1982).
25. Preservational biases may also have controlled the observed pattern of extinction. However, because there are more fossils in Units III and IV than in the upper 30 m of Unit I, we would expect to find the Permian taxa if they continued higher in the section. As that is not the case, we conclude that the observed ranges are real samples of the preservable fauna in the depositional basin.
26. M. S. Springer, Paleobiology 16, 512 (1990).
27. A. Solow, Paleobiology 29, 181 (2003).
28. C. R. Marshall, Paleobiology 20, 459 (1994).
29. S. Wang, C. R. Marshall, Paleobiology 30, 5 (2004).
30. G. H. Groenwald, J. W. Kitching, Geol. Surv. S. Afr. Biostratigraphy 1, 35 (1995).
31. G. M. King, S. Afr. Mus. Sidney Haughton Mem. Lect. 3, 1 (1990).
32. M. B. Steiner et al., Palaeogeogr. Palaeoclimatol. Palaeoecol. 194, 405 (2003).
33. There has been much recent criticism of the so-called P-T fungal spike as a chronostratigraphic marker, based on the discovery of multiple horizons at some localities and the complete absence of the marker at others, most notably at the important Greenland locality (39), as well as the possibility that the fossils may not have come from fungi at all (40).
34. L. Coney et al., L.P.S.C. 35, 1488 (2004).
35. N. C. Arens, A. H. Jahren, Palaios 15, 4 (2000).
36. P. Sheehan et al., Science 254, 835 (1991).
37. P. D. Ward et al., Science 289, 1740 (2000).
38. J. Botha, R. Smith, in preparation.
39. R. J. Twitchett et al., Geology 29, 351 (2001).
40. C. Foster, M. Stephenson, First Int. Conf. Palynology, Abst. 57 (2002).
41. We thank the NASA Astrobiology Institute, the NSF, and the National Research Foundation of South Africa for funding. Help in the field and fossil preparation came from the Karoo Paleontology Department, Iziko: South African Museum (P. October, H. Stumer, G. Farrell, preparation by A. Crean, field collection by N. Ward and T. Evans, and lab help by C. Converse and E. Steig). Paleomagnetic software used for data analysis was from C. Jones at the University of Colorado, Boulder. We thank F. Kyte and C. Looy for prereviews.

Supporting Online Material
www.sciencemag.org/cgi/content/full/1107068/DC1
Materials and Methods
Figs. S1 to S4
Tables S1 and S2
References

3 November 2004; accepted 3 January 2005
Published online 20 January 2005;
10.1126/science.1107068
Include this information when citing this paper.

Supplemental Information

ABRUPT AND GRADUAL EXTINCTION AMONG LATE PERMIAN LAND VERTEBRATES IN THE KAROO BASIN, SOUTH AFRICA

Peter D. Ward,* Jennifer Botha, Roger Buick, Michiel O. De Kock, Douglas H. Erwin, Geoffrey Garrison, Joseph Kirschvink, and Roger Smith

* To whom correspondence should be addressed . E-mail: argo@u.washington.edu

Paleomagnetic Measurement Methods

One previous paleomagnetic study of these sediments in the western portion of the Cape fold belt of Southern Africa revealed a pervasive remagnetization associated with Mesozoic deformation and the intrusion of dolerite dikes and sills (*1*); sediments along the margin of the Cape fold belt acquired their NRM after deformation of the strata, presumably as a result of thermochemical alteration. For our paleomagnetic studies we report results from three paleontologically well-constrained sections in the flat-lying Karoo well away from this fold belt which span the Permian/Triassic boundary. Two of these are in the vicinity of Lootsberg Pass (*2*), along each stretch of the highway, East and West of the summit, merging at the top. We also intensively sampled a 5m thick sequence of the Permian/Triassic 'Event beds" at Carlton Heights (*3*). In addition, results from a smaller section at Komandodriftam have been reported recently (*4*).

Paleomagnetic samples were obtained using standard techniques with gasoline powered drills and 2.5 cm diameter diamond coring bits. Cores were oriented *in situ* with a magnetic compass and, where possible, by sun compass. All samples were analyzed at

the California Institute of Technology paleomagnetics laboratory, using a 3-axis DC-SQUID moment magnetometer system housed in a magnetically shielded μ-metal room. The background noise of this instrument is less than 1 picoA·m^2, and it is equipped with a vacuum pick-and-put, computer-controlled sample handling system which can measure up to 180 samples automatically (*5*). AF demagnetization was performed with a computer-controlled, three-axis coil system. Thermal demagnetization was performed in a commercially-built magnetically shielded furnace.

All samples were initially measured for natural remnant magnetization, and then subjected to low AF demagnetization up to 10 mT at ~2 mT steps to remove low coercivity magnetizations. The samples were then treated with thermal demagnetization from 100°C in ~25° C increments to 525° C, in 15 or 20° C increments to 640° C, and when warranted, several more steps up to 688° C or until they became unstable (Fig. S1). Approximately 4,800 demagnetization experiments and associated magnetic measurements were performed on the 184 samples, or about 26 demagnetization steps per sample. In all but the low-field Af demagnetization steps, we used 8 sets of complete vector measurements (4 up-arrow, 4 down arrow) to assess the stability.

Three general rock types were analyzed in this study, blue-green claystone and sandstone, reddish claystone and sandstone, and the medium-grained dolerite dikes that intrude throughout the Karoo (*6*). The majority of samples could be characterized as well-behaved, with most possessing a component of low Af and thermal stability similar to the present magnetic field direction in Southern Africa, as well as one or two additional components of higher thermal stability. Demagnetization data were analyzed using principal component analysis to isolate stable magnetic directions (*7*) and to assess the

polarity of samples with multiple components. Only demagnetization lines with MAD values below 10°, and planes below 15°, were included in the statistical analysis. Mean directions were obtained using Fisher statistics (*8*), and the method of McFadden & McElhinny (*9*) was used for combining data from demagnetization lines and arcs, and the final iterative directions along the arc constraints were combined with lines for the stratigraphic polarity interpretation. The reversals test followed that of McFadden & McElhinny (*10*). Cleaned directional data from the sampling sites (Fig. S2) show a baked contact test near the base of the West Lootsberg Pass section.

Dolerite dikes of the Karoo intrusive complex (*6*) are present in the Lootsberg pass area, but appear absent at the Carlton Heights locality. West Lootsberg Pass has a single vertical dike ~4 m thick, which crosses the section three times, once at the ~ 15 m level in the stream cut near the bottom of the section, again in the road cut near the ~160 meter level, and once again at the summit of the combined East and West Lootsberg Pass sections (Fig. S3). Fossil bone samples collected away from this intrusion are light in color, but within ~10m of the dike they darken progressively. Demagnetization experiments on samples of the dolerite isolate a consistent Southeast and shallow magnetic direction, nearly 40 degrees away from that of either the expected Permo-Triassic reversed field for southern Gondwana (*11*) or the mean direction in the Karoo intrusive suite (*6*). This is fortuitous, as this angular separation is enough to permit reliable identification of the dolerite-induced remagnetization direction in the Lootsberg Pass samples. This also implies that the time scale for the emplacement of the intrusion in this area was short relative to the time scale of secular variation, as all units in the Pass area yield essentially the same direction. Figure S1 shows examples of the

demagnetization behavior of three of the red siltstone samples which have been partially or totally remagnetized by this intrusion near the base of the West Lootsberg Pass section. At low demagnetization steps a present field component is removed, and the magnetic vectors follow great circle arcs headed towards the dolerite direction on the equal-area projections. At higher temperatures, however, magnetic vectors in the two samples furthest from the intrusion change their trajectory and move on similar great-circle arcs towards the Permo/Triassic normal polarity direction. The demagnetization temperature at which this happens decreases with distance from the intrusion, as is expected from a thermomagnetic overprint. The sample closest to the sill has been remagnetized entirely. This constitutes a positive baked contact test for the high-temperature component (*12*), indicating that it predates intrusion of the dolerite. Unfortunately, most of the greenish samples are located in the stream exposures in the lower part of the section, and appear to have been remagnetized by the intrusion. Note that at Komandodriftam, both the greenish and reddish sediments are capable of preserving primary directions, if free from surface weathering (*4*).

Careful thermal demagnetization experiments on the reddish samples in the temperature range from 550 to 688°C usually yields clear great-circle arcs towards either the Permo/Triassic normal or reversed directions, which commonly end in a stable direction. The two groups of directions pass the reversals test with a "B" classification (*10*) as indicated in Table S1.

The major problem in the paleomagnetic studies described here and by De Kock & Kirschvink (*4*) is the ability to distinguish the Karoo Permian-Triassic Normal direction from that of the Present Local Field, (PLF), which are separated by an angular

distance of only 15º, implying that the scatter cones of their Fisherian distributions overlap. At first, this problem appears somewhat intractable, as the sediments are essentially flat-lying and the present field overprint is pervasive. However, at the Lootsberg pass locality it became clear during examination of the Normally magnetized interval approaching the basal dolerite sill mentioned above that the weathering effects were, in general, removed at the lower Af and thermal demagnetization steps (≤ 400° C). This PLF component had essentially intruded upon the portion of the stability spectrum that had been remagnetized by the intrusion. Above these temperatures it was usually possible to observe motion of the NRM vector towards a high-temperature, Permian/Triassic Boundary (PTB) Normal direction (Fig. S2). These components could either be isolated by principal component analysis on the high-temperature steps, or via the use of great-circle arc constraints as noted above. Examination of the samples higher up in this sequence reveal that the same technique also works on those samples interpreted to be in the Reversed polarity interval, with small arcs moving away from the Present direction towards the SE and down PTB Reversed direction. Figure S2 shows the arc constraints on these directions. This approach tends to be conservative for the Normal polarity directions, as those samples that contain a primary component too similar to that of the present field direction (no directional change in position with demagnetization) are simply not used in the analysis. Although this occasional exclusion does bias the mean group of Normal directions slightly away from the true mean, and is the probable cause of the slight deviation from antiparallelism in the Normal and Reversed polarity groups shown on Table S1, the polarity interpretation is conservative.

A clear stratigraphic distinction exists in these sections, and all samples below the 130 m mark at Lootsberg West display normal polarity and those above show only reversed polarity (Fig. S3), with the exception of a small group of samples above the point where these two sections merge. In conjunction with the reversal (R/N) found by De Kock & Kirschvink (*4*) at the Komandodriftdam locality, which is slightly below the P/T boundary event beds (*13*), this yields a pattern of four magnetic polarity Chrons, which we are designating R1/N1/R2/N2. The P/T boundary, as determined from vertebrate paleontology, lies above the base of Chron N1. We interpret our Chron N1 to be correlative to the basal Triassic Normal Chron identified in many other parts of the world, in both marine and terrestrial sediments (*14, 15*), but we note with some dismay that this marine extinction horizon has been suggested to be either near the base of this Normal Chron, as it is here, or in the uppermost portion of the underlying Reversed Chron (see (*16*) for a discussion).

The combination of the baked contact test, the reversals test, and the presence of layer-bound magnetic polarity zones strongly implies that the magnetization was acquired at or shortly after the time of deposition. Given the robust number of samples yielding useable results, and the excellent age constraints on the Permian/Triassic boundary (*17, 18*), the mean direction rates a perfect 7 on the 7-point paleomagnetic quality (Q) index of Van der Voo (*19*), and indicates a paleolatitude of ~ 41° S.

Table S1. Summary of paleomagnetic Fisherian statistics from the Lootsberg Pass and Carlton Heights sections. No structural correction has been made because the sediments are flat-lying. Data for the dolerite overprint direction include samples from the dike as well as remagnetized sediments. 'N_{eff}' indicates the effective number of samples in the

analysis, and (L, P) give the number of individual demagnetization Lines and Planes, respectively (N_{eff} = L + ½P; see (*9*)) . As separate groups, the Normal and Reversed directions pass the paleomagnetic reversals test with "B" classification (*10*). The summit of Lootsberg Pass, South Africa, is located at 31° 50.133' S, 24° 51.607' E, and Carlton Heights is at 31° 19.898' S, 24° 58.521' E. Raw demagnetization data, least-squares tables, and sample-by-sample interpretations will be posted at http://www.gps.caltech.edu/MagLab/ before publication.

East & West Lootsberg Pass, and Carlton Heights

	N(eff.)	(L, P)	Decl.	Incl.	α95	κ
PLF, overprint	93.0	(93, 0)	335.8	-59.3	1.7	76.46
OVP, dolerite overprint	37.5	(33, 9)	117.4	13.6	3.7	41.23
NOR, primary	45.5	(41,9)	303.3	-61.0	4.0	28.36
REV, primary	25.5	(5, 41)	133.1	57.1	4.3	46.27
NOR+REV	71.0	(46, 50)	307.1	-59.8	3.0	32.53

The pole is at 47.1 N, 267.6 E, (dp, dm) = (2.4, 4.5), paleolatitude -40.7 (-34.7/-44.2)

Komandodrift-dam (De Kock & Kirschvink, 2004)

	N(eff.)	(L, P)	Decl.	Incl.	α95	κ
NOR + REV	21.0	(7, 28)	311.9	-61.6	7.6	17.80

The mean directions from these studies are not statistically distinguishable (Gr = 0.8, Chi^2 p. value 0.668)

Supplemental Paleomagnetics References:

1. V. Bachtadse, R. Vandervoo, I. W. Halbich, *Earth and Planetary Science Letters* **84**, 487 (1987).
2. G. H. Groenewald, J. W. Kitching, in *Biostratigraphy of the Beaufort Group (Karoo Supergroup)* B. S. Rubidge, Ed. (Council for Geosciences, South African Committee for Stratigraphy, Geological Society of South Africa, 1995), vol. 1, pp. 35-39.
3. M. B. Steiner, Y. Eshet, M. R. Rampino, D. M. Schwindt, *Palaeogeography Palaeoclimatology Palaeoecology* **194**, 405 (May 25, 2003).
4. M. O. De Kock, J. L. Kirschvink, *Gondwana Research* **7**, 175 (2004).
5. J. L. Kirschvink, paper presented at the Spring AGU Meeting, Boston, MA 2002.

6. R. B. Hargraves, J. Rehacek, P. R. Hooper, *South African Journal of Geology* **100**, 195 (1997).
7. J. L. Kirschvink, *Geoph. J. Royal Astr. Soc.* **62**, 699 (1980).
8. R. A. Fisher, *Porc. R. Soc. A* **217**, 295 (1953).
9. P. L. Mcfadden, M. W. McElhinny, *Earth & Planetary Science Letters* **87**, 161 (1988).
10. P. L. McFadden, M. W. McElhinny, *Geophysical Journal Int.* **103**, 725 (1990).
11. F. Torq, e. al., *Earth and Planetary Science Letters* **148**, 553 (1997).
12. R. F. Butler, *Paleomagnetism : magnetic domains to geologic terranes* (Blackwell Scientific Publications, Boston, 1992), pp. 319.
13. R. M. H. Smith, P. D. Ward, *Geology* **29**, 1147 (Dec, 2001).
14. M. Szurlies, G. H. Bachmann, M. Menning, N. R. Nowaczyk, K. C. Kading, *Earth and Planetary Science Letters* **212**, 263 (Jul 25, 2003).
15. M. Steiner, J. Ogg, Z. Zhang, S. Sun, *J. Geophysical Research* **94**, 7343 (1989).
16. J. Nawrocki, *Terra Nova* **16**, 139 (Jun, 2004).
17. S. A. Bowring *et al.*, *Science* **280**, 1039 (May 15, 1998).
18. P. R. Renne, Z. C. Zhang, M. A. Richards, M. T. Black, A. R. Basu, *Science* **269**, 1413 (Sep 8, 1995).
19. R. Van der Voo, *Palaeomagnetism of the Atlantic, Tethys, and Iapetus Oceans* (Cambridge University Press, Cambridge, U.K., 1993), pp. 411.
20. P. D. Ward, D. R. Montgomery, R. Smith, *Science* **289**, 1740 (Sep 8, 2000).

Figure S1. Demagnetization data for the baked contact test. Samples BGLP- 179, 180, and 181 are red siltstones collected from near the base of the West Lootsberg Pass section where it approaches the vicinity of the dolerite dike, as indicated on Fig. S3. On the equal area diagrams here the solid (open) symbols indicate downwards (upwards) magnetic directions. On the orthogonal projections, the red symbols indicate projection of the remanence vector into the horizontal plane, and blue symbols are the corresponding projection into the East/West vertical plane. The high-temperature component becomes progressively weaker, and the dolerite overprint component stronger, as the sampling locality approaches the dike.

Figure S2. Equal-area plots showing the principal magnetic components isolated from the demagnetization data generated in this study. Directions obtained from linear components are shown as squares, and the arc-segments show the constraints from demagnetization planes (*9*). Overprint directions shown on the left-hand diagram include those attributed to chemical and viscous remagnetization during weathering in the present geomagnetic field, and that of the mid-Mesozoic field which was present during the intrusion and cooling of the dolerite sill. The right-hand diagram shows the high-temperature, two polarity component interpreted as the primary Permo-Triassic field direction. Although the mean Normal polarity P/T direction is similar to that of the present field overprint, they are separated easily by the large difference in their thermal stability properties as shown on Fig. S1. Statistical data for these components are given in Table S1.

Figure S3. Range data for Permian and lower Triassic strata in Karoo basin, compiled from ref 16 and the new data presented here. Each taxon is a genus. This graph supports

our contention that significant background extinction was occurring well before the P/T event. While no equivalent graph plotted such as that presented here exists for the Hell Creek formation (with a time span of about half that shown in the Permian part of this diagram), the work of (*9*) has demonstrated that at least among dinosaurs there no decrease in taxa prior to the K/P event occurred.

Supplemental Materials: Stable Isotopic Measurement Methods

Inorganic carbonate $\delta^{13}C$ ($\delta^{13}C_{carb}$) data comes from paleosol carbonate nodules, while the bulk sedimentary organic carbon isotope record ($\delta^{13}C_{org}$) comes from fine-grained pond and overbank deposits. Carbonate soil nodule ^{13}C:^{12}C ratios are controlled by temperature and pore space $\delta^{13}C_{CO2}$. Pore space $\delta^{13}C_{CO2}$ is controlled by both the CO_2 produced *in situ* from the microbial remineralization of buried organic matter (i.e., respired CO_2), and atmospheric CO_2 diffusing into the soil. Thus, the nodule $\delta^{13}C_{carb}$ ratio is affected not only by the $\delta^{13}C_{CO2}$ but also the partial pressure of CO_2 (pCO_2) in the atmosphere; a negative excursion in soil nodule $\delta^{13}C_{carb}$ can be caused by both a decrease in $\delta^{13}C_{CO2}$ and an increase in atmospheric pCO_2. Sedimentary organic ^{13}C:^{12}C ($\delta^{13}C_{org}$) was analyzed via elemental analyzer–continuous-flow isotope ratio mass spectrometry (EACFIRMS) at the Stable Isotope Research Facility (SIRF); SIRF is operated jointly by the Quaternary Research Center and the Astrobiology Program at the University of Washington. Powdered samples were first acidified with >5 ml 10% HCl per mg of sample material and kept at 40°C for at least 12 hr to remove inorganic carbonate material. Samples were then triple rinsed with ultrapure (>18 MΩ) deionized

water and oven dried at 40°C. Total carbonate removal by this procedure was verified by measuring $\delta^{13}C_{org}$ during a series of repeated acid leaching tests on six samples from the Lootsberg section (Fig. S5). Analyses were made with a Costech ECS 4010 Elemental Analyzer coupled to a ThermoFinnigan MAT253 mass spectrometer via a ThermoFinnigan CONFLO III gas interface. Carbonate mineral ^{13}C:^{12}C ($\delta^{13}C_{carb}$) and ^{18}O:^{16}O ($\delta^{18}O_{carb}$) were measured by IRMS on a Micromass Isoprime dual inlet mass spectrometer. Samples were introduced via a Micromass carbonate autosampler system. Samples were held in evacuated 5 ml vacutainers with proprietary CO_2-impermeable seals and acidified with 103% phosphoric acid at 90°C for 10 minutes; the evolved CO_2 was cryogenically stripped of water vapor prior to being introduced to the mass spectrometer. Isotope ratios are reported in standard delta (δ) notation relative to Vienna Pee Dee Beleminite (VPDB), where $\delta^{13}C = [[(^{13}C/^{12}C)\ sample/(^{13}C\ /^{12}C)\ VPDB]-1]*1000$; internal laboratory reference materials for $\delta^{13}C$ and $\delta^{18}O$ analyses have been calibrated against NBS-19 (calcite; $\delta^{13}C$ = +1.95‰, $\delta^{18}O$ = -2.20‰, VPDB). The standard deviation (σ) of sample replicates was 0.15‰ for $\delta^{13}C_{org}$ (n = 36), 0.10‰ for $\delta^{13}C_{carb}$ (n = 50), and 0.25‰ for $\delta^{18}O_{carb}$ (n = 50). Analytical precision based on routine analyses of internal laboratory reference materials was 0.15‰ for $\delta^{13}C_{org}$ and 0.21‰ for $\delta^{13}C_{carb}$ and $\delta^{18}O_{carb}$.

Results from tests of our carbonate removal techniques. (a) $\delta^{13}C_{org}$ vs. increasing ml 10% HCl:mg sample ratio of six samples taken from the Lootsberg section. Three mg of 10% HCl per mg of sample was considered the minimum acid:sample ratio to remove carbonate material from the samples. (b) $\delta^{13}C_{org}$ vs. heating duration of the same samples in (a) having been treated with 4 ml 10% HCl per ug of sample material. Twenty-four hours was considered enough time at 40°C to remove any recalcitrant carbonate mineral phases such as siderite and dolomite.

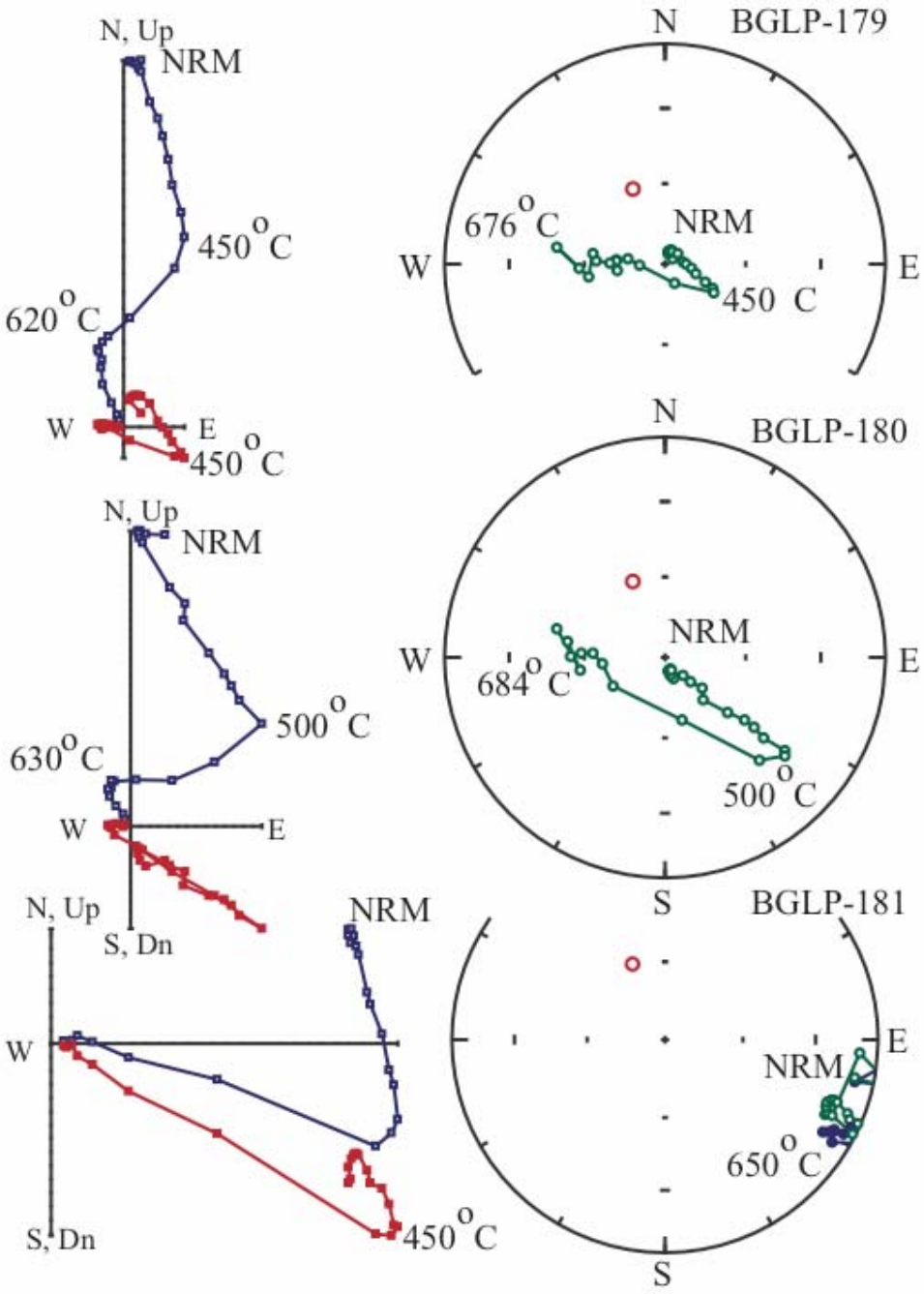

Fig. S1, Ward et al.

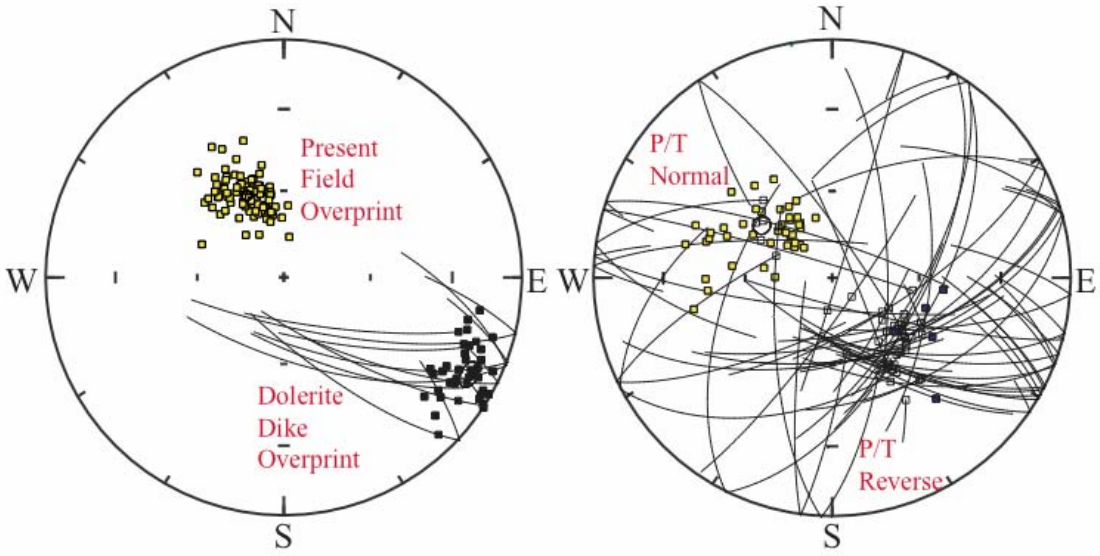

Fig. S2 Ward et al.

a. **b.**

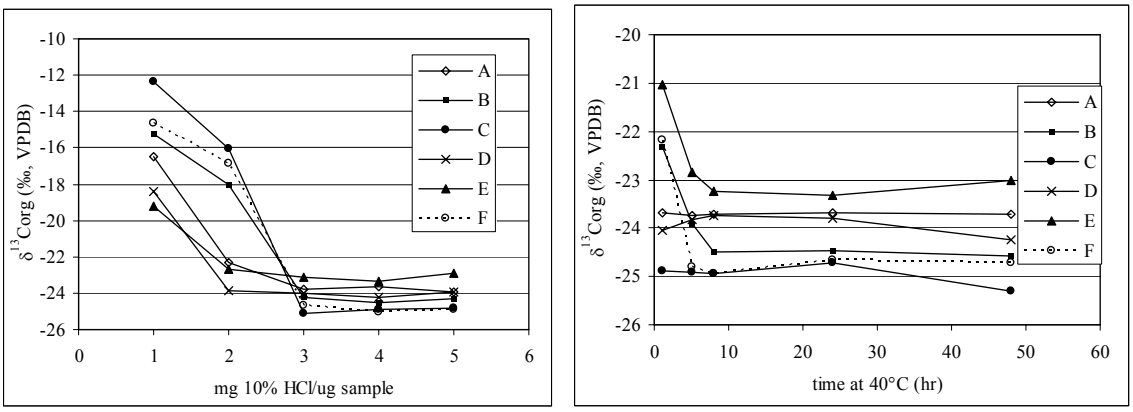

Figure S3 Ward et al.

Table S2. Sedimentary stable carbon isotope data

WAPATS BERG						BETHULIE					CARLTON HEIGHTS					LOOTSBERG				
ID1	ID2	Strat. position (m)	No. of analyses	δ^{13}Corg (‰, VPDB)	SD	ID	Strat. position (m)	No. of analyses	δ^{13}Corg (‰, VPDB)	SD	ID	Strat. position (m)	No. of analyses	δ^{13}Corg (‰, VPDB)	SD	ID	Strat. position (m)	No. of analyses	δ^{13}Corg (‰, VPDB)	SD
11/21/01	47	25.5	1	-24.04		26	19.6	2	-24.18	1.13	61	36.9	1	-22.89		49	34.6	4	-23.63	0.03
11/21/01	46	22.2	1	-24.54		25	19.45	2	-23.85	0.29	60	35.1	3	-22.73	0.24	47	33.3	3	-22.19	0.17
11/21/01	45	19.9	1	-24.31		24	18.8	2	-23.30	0.11	59	34.45	2	-23.36	0.00	46	32.9	2	-21.63	0.36
11/21/01	44	18.75	1	-24.19		23	18.05	2	-23.66	0.22	58	33.5	3	-23.26	0.34	45	32.2	4	-21.85	0.52
11/21/01	43	17.85	2	-24.29	0.11	22	17.3	2	-23.80	0.14	57	32.5	2	-23.51		44	31.2	2	-21.82	0.60
11/21/01	42	16.2	2	-24.95	0.44	21	16.7	2	-23.29	0.10	56	31.7	2	-23.63	0.53	43	30.15	2	-22.61	0.11
11/21/01	41	15	1	-24.35		20	15.3	2	-23.40	0.01	55	30.9	3	-22.65	0.24	42	29.5	2	-22.38	0.00
11/21/01	40	14	2	-24.26	0.28	19	14.2	2	-23.31	0.06	54	28	3	-22.67	0.04	41	28.7	4	-23.42	0.06
11/21/01	39	13.05	2	-23.33	0.61	18	13.3	2	-23.31	0.10	53	27	2	-22.88	0.00	40	27.65	4	-22.02	1.06
11/21/01	38	12.5	1	-23.41		17	12.1	2	-22.76	0.11	52	26.15	2	-22.53	0.00	39	27.15	3	-22.08	0.25
11/21/01	37	11.95	1	-24.12		16	11.1	2	-23.16	0.52	51	25.3	1	-23.36		38	26.9	2	-22.59	0.08
11/21/01	36	11.25	1	-23.83		15	10.2	2	-23.30	0.06	50	24.35	3	-22.77	0.19	37	22.35	4	-21.95	0.38
11/21/01	35	10.85	1	-23.38		14	8.6	2	-23.34	0.31	49	24.05	3	-22.64	0.11	36	22.2	2	-21.96	0.90
11/21/01	33	10.3	1	-23.13		13	8.1	1	-24.03		48	23.1	3	-22.61	0.03	35	21.35	3	-21.55	0.58
11/21/01	32	10.1	1	-23.43		12	7.35	2	-23.10	0.34	47	22.8	3	-22.81	0.24	34	20.05	4	-22.54	0.45
11/21/01	31	9.9	1	-23.32		11	6.8	2	-24.73	0.29	46	21.4	3	-23.01	0.07	33	20.00	4	-23.17	1.11
11/21/01	29	9.45	1	-22.87		10	4.15	2	-24.28	0.47	44	20	2	-22.98		32	18.45	2	-24.74	0.01
11/21/01	28	9.15	1	-23.70		9	3.5	3	-22.95	0.39	43	19.9	3	-22.55	0.15	31	17.7	2	-24.28	0.09
11/21/01	27	8.45	3	-24.04	0.77	8	2.75	2	-22.79	0.03	42	19.1	2	-22.35		30	17.4	2	-24.80	0.06
11/21/01	26	7.9	1	-24.89		7	2.05	2	-23.57	0.05	3	18.8	2	-23.23	0.29	29	17	2	-24.94	0.08
11/21/01	25	7.1	3	-23.17		6	1.4	2	-23.85	0.10	4	18.7	3	-23.68	0.25	28	15.1	3	-24.34	0.00
11/21/01	24	6.4	3	-22.95	0.51	5	1.15	2	-24.11	0.83	5	18.55	2	-24.71	0.58	27	13.55	2	-25.10	0.16
11/21/01	23	5.9	3	-22.46	0.90	4	0.85	1	-24.55		9	17.85	4	-23.81	0.20	25	10.7	2	-25.38	0.45
11/21/01	22	5.45	4	-24.41	0.03	3	0.4	2	-23.69	0.13	10	17.6	2	-23.58	0.44	24	10	2	-24.56	0.36
11/21/01	21	5.05	2	-23.94	0.35	2	0	2	-23.75	0.06	11	17.15	2	-23.66	0.12	23	8.45	2	-24.67	0.28
11/21/01	20	4.75	2	-24.16	0.82	1	-0.01	3	-23.49	0.22	12	16.65	1	-23.51		22	8.25	1	-24.97	
11/21/01	16	4.55	2	-22.86		27	-0.35	2	-23.61	0.12	13	16.3	1	-23.97		21	7.8	6	-24.98	0.93
11/21/01	15	4.25	2	-22.75		28	-1.25	3	-24.07	0.51	14	15.95	2	-24.35	0.47	20	6.35	4	-24.48	0.66
11/21/01	14	3.9	2	-23.84	0.79	32	-1.65	2	-23.52	0.01	15	15.7	3	-24.10	0.23	19	6.05	4	-24.94	0.79
11/21/01	13	3.35	2	-23.77	0.56	29	-1.8	3	-23.45	0.59	16	14.9	2	-25.30	0.15	18	5.6	2	-24.39	0.34
11/21/01	12	3.15	2	-24.63	0.24	30	-2.65	2	-23.78	0.22	17	14.45	3	-24.46	0.39	17	4.7	3	-22.50	0.11
11/21/01	11	2.95	5	-24.30	0.63	31	-3.5	2	-24.13	0.03	18	14.15	1	-23.80		16	4.3	4	-23.63	0.76
11/21/01	10	2.6	4	-25.19	0.35	33	-6	2	-24.35	0.10	20	13.05	4	-24.13	0.12	14	3.3	4	-24.36	0.30
11/21/01	9	2.35	3	-24.64	0.47	34	-7.65	2	-22.77	0.25	21	11.95	2	-23.44	0.00	13	3	2	-25.02	0.21
11/21/01	8	2.1	4	-24.16		35	-9.4	2	-23.43	0.06	22	11	4	-25.42	0.19	12	2.75	3	-23.62	0.83
11/21/01	7	1.65	2	-23.79	0.29	36	-11.1	3	-23.57	0.23	23	10.35	4	-24.04	0.21	10	2.25	2	-24.69	0.46
11/21/01	6	1	4	-23.41	0.23	37	-12.4	4	-23.64	0.43	24	9.75	4	-25.32	0.31	9	2	1	-24.78	
11/21/01	5	0.8	1	-23.18		38	-13.8	2	-23.69	0.32	25	8.95	4	-24.52	0.30	8	1.75	2	-24.48	0.34

WAPATS BURG

ID#1	ID#2	Strat. position (m)	No. of analyses	δ^{13}Corg (‰, VPDB)	SD
11/21/01	1a	0.5	1	-22.74	
11/21/01	3	0.4	5	-23.00	0.34
11/21/01	2	0.15	4	-23.18	0.53
11/20/01	2	0	2	-25.76	0.59
11/21/01	17	-0.2	3	-22.90	0.55
11/21/01	18	-0.4	2	-23.34	0.55
11/20/01	3	-0.55	2	-25.51	0.55
11/21/01	19	-0.75	5	-23.71	1.20
11/20/01	4	-0.9	2	-24.96	0.18
11/20/01	5	-1.35	4	-23.40	0.34
11/20/01	6	-2.1	2	-24.28	0.08
11/20/01	7	-2.55	2	-23.97	0.09
11/20/01	8	-3.15	2	-23.38	0.23
11/20/01	9	-3.8	2	-23.75	0.08
11/20/01	10	-5.15	2	-24.02	0.05
11/20/01	12	-6.25	2	-25.46	0.16
11/20/01	13	-7	2	-23.96	0.38
11/20/01	14	-8	2	-23.73	0.01
11/20/01	15	-9.05	2	-24.33	0.26
11/20/01	16	-10.3	2	-23.35	0.15
11/20/01	17	-11.9	2	-24.22	0.40
11/20/01	18	-12.7	2	-23.63	0.11
11/20/01	19	-16.05	2	-24.27	0.67
11/20/01	20	-16.85	2	-23.83	0.14
11/20/01	21	-18.05	1	-23.17	

BETHULIE

ID	Strat. position (m)	No. of analyses	δ^{13}Corg (‰, VPDB)	SD
41	-17.2	2	-23.12	0.06
42	-18.8	2	-22.40	0.00
43	-20	2	-22.49	0.15

CARLTON HEIGHTS

ID	Strat. position (m)	No. of analyses	δ^{13}Corg (‰, VPDB)	SD
30	5.7	1	-25.08	
31	4.8	2	-24.29	0.45
32	4	1	-22.62	
33	2.75	3	-23.96	0.33
36	1.1	1	-24.66	
37	0.6	2	-23.90	0.48
38	0.3	2	-23.04	0.11
39	0	1	-22.17	
40	-0.3	2	-23.99	0.31
41	-0.75	2	-22.44	0.16

Figure S4. Range data for Permian and lower Triassic strata in Karoo Basin, compiled from ref 16 and the new data presented here. Each taxon is a genus. This graph supports our contention that significant background extinction was occurring well before the P/T event. While no equivalent graph plotted such as that presented here exists for the Hell Creek formation (with a time span of about half that shown in the Permian part of this diagram), the work of (*9*) has demonstrated that at least among dinosaurs there no decrease in taxa prior to the K/P event occurred.

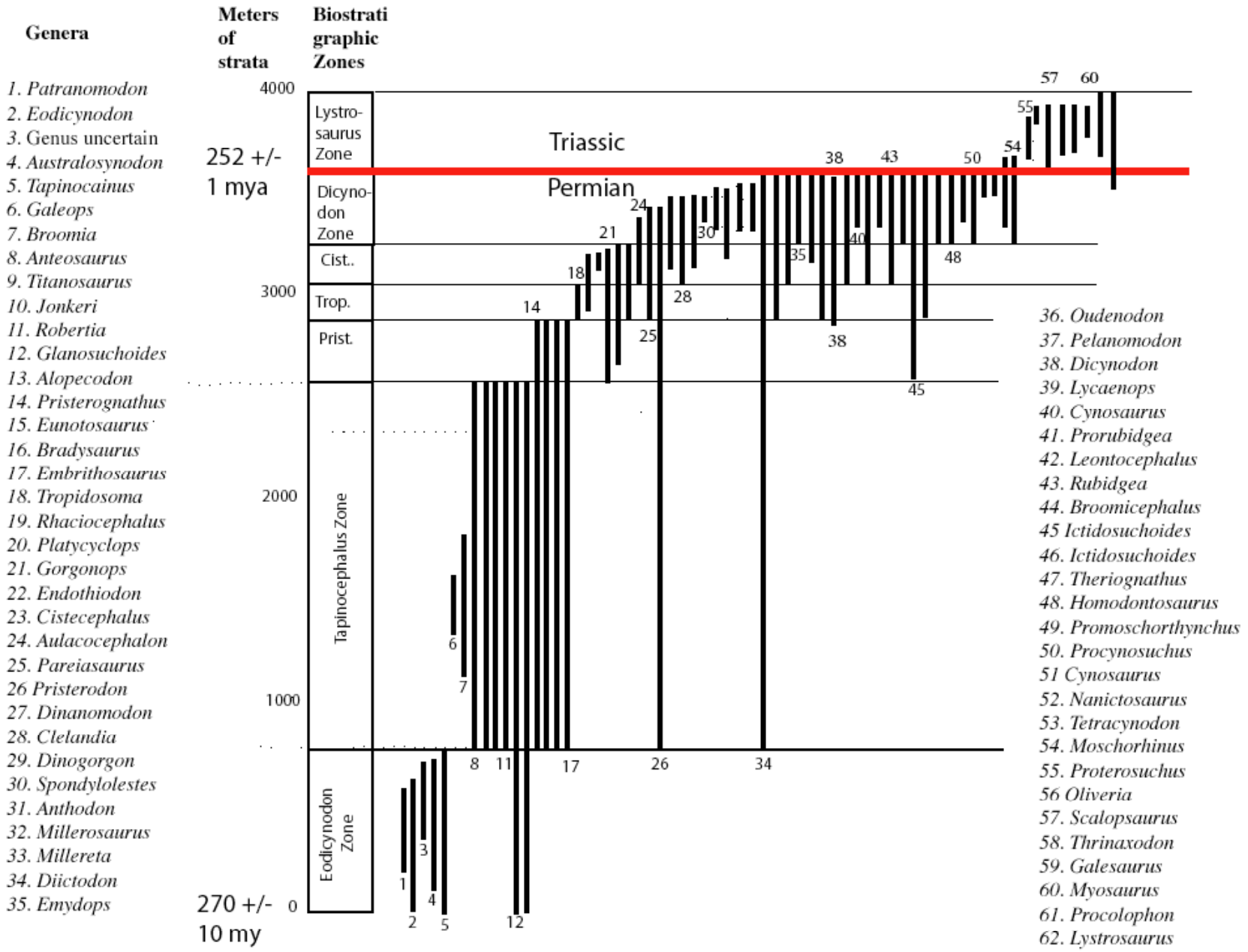
Genera
1. Patranomodon
2. Eodicynodon
3. Genus uncertain
4. Australosynodon
5. Tapinocainus
6. Galeops
7. Broomia
8. Anteosaurus
9. Titanosaurus
10. Jonkeri
11. Robertia
12. Glanosuchoides
13. Alopecodon
14. Pristerognathus
15. Eunotosaurus
16. Bradysaurus
17. Embrithosaurus
18. Tropidosoma
19. Rhaciocephalus
20. Platycyclops
21. Gorgonops
22. Endothiodon
23. Cistecephalus
24. Aulacocephalon
25. Pareiasaurus
26 Pristerodon
27. Dinanomodon
28. Clelandia
29. Dinogorgon
30. Spondylolestes
31. Anthodon
32. Millerosaurus
33. Millereta
34. Diictodon
35. Emydops
Meters of strata
Biostratigraphic Zones
4000
3000
2000
1000
0
252 +/- 1 mya
270 +/- 10 my
Lystro-saurus Zone
Dicyno-don Zone
Cist..
Trop.
Prist.
Tapinocephalus Zone
Eodicynodon Zone
Triassic
Permian
36. Oudenodon
37. Pelanomodon
38. Dicynodon
39. Lycaenops
40. Cynosaurus
41. Prorubidgea
42. Leontocephalus
43. Rubidgea
44. Broomicephalus
45 Ictidosuchoides
46. Ictidosuchoides
47. Theriognathus
48. Homodontosaurus
49. Promoschorthynchus
50. Procynosuchus
51 Cynosaurus
52. Nanictosaurus
53. Tetracynodon
54. Moschorhinus
55. Proterosuchus
56 Oliveria
57. Scalopsaurus
58. Thrinaxodon
59. Galesaurus
60. Myosaurus
61. Procolophon
62. Lystrosaurus